ZEUS-prel-05-008-plus

Submitted to the
XXXIII International Conference on High Energy Physics
July 26 - August 2, 2006, Moscow, Russia

Abstract: -

Session: QCD hard interactions
Heavy Quark physics

Measurement of beauty production from dimuon events at HERA

ZEUS Collaboration

20 July 2006

Abstract

Beauty production with events in which two muons are observed in the final state has been measured with the ZEUS detector at HERA using an integrated luminosity of 114 pb^{-1}. A low p_T threshold for muon identification, in combination with the large rapidity coverage of the ZEUS muon system, gives access to essentially the full phase space for beauty production. The total cross section for beauty production in ep collisions at $\sqrt{s} = 318$ GeV has been measured, $\sigma_{\rm tot}(ep \to b\bar{b}X) = 16.1 \pm 1.8(\text{stat.})^{+5.3}_{-4.8}(\text{syst.})$ nb. Differential cross sections and a measurement of $b\bar{b}$ correlations are also obtained, and compared to other beauty cross section measurements, MC models and NLO QCD predictions. The latter agree with the data within errors, but tend to lie below the measurements. The shapes of all distributions are well described.

1 Introduction

The production of beauty quarks in ep collisions at HERA is a stringent test for perturbative Quantum Chromodynamics (QCD) since the large b-quark mass ($m_b \sim 5\,\mathrm{GeV}$) provides a hard scale that should ensure reliable predictions in all regions of phase space, including the kinematic threshold region. In this region, with b-quark transverse momenta comparable to or less than the b-quark mass, next-to-leading-order (NLO) QCD calculations in which the (massive) b quarks are generated dynamically are expected to provide accurate predictions [1, 2].

The beauty-production cross section has been measured in $p\bar{p}$ collisions at the S$p\bar{p}$S [3] and Tevatron colliders [4], in $\gamma\gamma$ interactions at LEP [5], and in fixed-target πN [6] and pN [7] experiments. While most results, including recent results from the Tevatron, are in good agreement with QCD predictions, some, in particular those from LEP from photon-photon fusion, show large discrepancies.

Most previous measurements of beauty production at HERA selected beauty events by requiring the presence of one or more jets, tagged by a muon or electron from the semi-leptonic decay of one of the beauty quarks [8–11], or by tracks originating from the secondary decay vertex of beauty hadrons [12]. This restricts the measurements to high p_T b quarks.

This paper reports measurements of beauty production via the reaction $ep \to b\bar{b}X \to \mu\mu X'$ using the ZEUS detector at HERA. The dimuon final state yields a data sample enriched in $b\bar{b}$ pairs, and with strongly suppressed backgrounds from other processes. This allows low p_T^μ thresholds to be applied without any jet requirements, and yields sensitivity to a larger region of phase space, especially towards lower transverse momenta of the b quarks.

Conceptually, the analysis is similar to the analysis of beauty in $D^*\mu$ final states [13, 14], with three significant differences. The larger branching ratio yields higher statistics, so that differential cross sections can be measured. The wider rapidity coverage and very low p_T threshold allow the extraction of the total beauty cross section with almost no extrapolation. The low charm background allows measurements of $b\bar{b}$ correlations, testing the influence of higher order contributions on the perturbative calculations.

2 Experimental set-up

The data sample used in this analysis corresponds to an integrated luminosity $\mathcal{L} = 114.1 \pm 2.3\ \mathrm{pb}^{-1}$, collected by the ZEUS detector in the years 1996-1997 and 1998-2000. During the 1996-97 data taking, HERA provided collisions between an electron[1] beam of $E_e = 27.5\,\mathrm{GeV}$ and a proton beam of $E_p = 820\,\mathrm{GeV}$, corresponding to a centre-of-mass energy $\sqrt{s} = 300\,\mathrm{GeV}$ ($\mathcal{L}_{300} = 38.0 \pm 0.6$ pb^{-1}). In the years 1998-2000, the proton-beam energy was $E_p = 920\,\mathrm{GeV}$, corresponding to $\sqrt{s} = 318\,\mathrm{GeV}$ ($\mathcal{L}_{318} = 76.1 \pm 1.7$ pb^{-1}).

A detailed description of the ZEUS detector can be found elsewhere [15]. A brief outline of the components that are most relevant for this analysis is given below.

Charged particles are tracked in the central tracking detector (CTD) [16], which operates in a magnetic field of 1.43 T provided by a thin superconducting coil. The CTD consists of 72 cylindrical drift chamber layers, organized in 9 superlayers covering the polar-angle[2] region $15^\circ < \theta < 164^\circ$. The transverse-momentum resolution for full-length tracks is $\sigma(p_T)/p_T = 0.0058 p_T \oplus 0.0065 \oplus 0.0014/p_T$, with p_T in GeV.

The high-resolution uranium–scintillator calorimeter (CAL) [17] consists of three parts: the forward (FCAL), the barrel (BCAL) and the rear (RCAL) calorimeters. Each part is subdivided transversely into towers and longitudinally into one electromagnetic section (EMC) and either one (in RCAL) or two (in BCAL and FCAL) hadronic sections (HAC). The smallest subdivision of the calorimeter is called a cell. The CAL energy resolutions, as measured under test-beam conditions, are $\sigma(E)/E = 0.18/\sqrt{E}$ for electrons and $\sigma(E)/E = 0.35/\sqrt{E}$ for hadrons (E in GeV).

The muon system consists of rear, barrel (R/BMUON) [18] and forward (FMUON) [19] tracking detectors. The B/RMUON consists of limited-streamer (LS) tube chambers placed behind the BCAL (RCAL), inside and outside the magnetised iron yoke surrounding the CAL. The barrel and rear muon chambers cover polar angles from 34° to 135° and from 135° to 171°, respectively. The FMUON consists of six trigger planes of LS tubes and four planes of drift chambers covering the angular region from 5° to 32°. The muon system exploits the magnetic field of the iron yoke and, in the forward direction, of two iron toroids magnetised to 1.6 T to provide an independent measurement of the muon momentum.

Muons are also detected by the sampling Backing Calorimeter (BAC) [20] This detector consists of 5200 aluminium proportional drift chambers which are typically 5 m long and have a wire spacing of 1 cm. The chambers are inserted into the iron yoke of the ZEUS detector (barrel and two end caps) covering the CAL. It is equipped with analogue (for

[1] Electrons and positrons are not distinguished in this paper and are both referred to as electrons.

[2] The ZEUS coordinate system is a right-handed Cartesian system, with the Z axis pointing in the proton beam direction, referred to as the "forward direction", and the X axis pointing left towards the centre of HERA. The coordinate origin is at the nominal interaction point. The pseudorapidity is defined as $\eta = -\ln\left(\tan\frac{\theta}{2}\right)$, where the polar angle, θ, is measured with respect to the proton beam direction.

energy measurement) and digital (for muon tracking) readouts. The former is based on 2000 towers (50×50 cm^2) providing an energy resolution of $\sim 100\%/\sqrt{E}$. The digital information on hit wires allows the reconstruction of muon trajectories in two dimensions (XY in barrel, YZ in end caps) with an accuracy of a few mm.

3 Principle of the measurement

Two principal event classes contribute to the beauty signal to be measured. The first of this is events in which the two muons originate from the same parent B hadron, e.g. through the sequential decay chain $b \to c\mu X \to s\mu\mu X'$. These yield unlike-sign muon pairs produced in the same event hemisphere and are constrained to dimuon invariant masses of $m_{\rm inv}^{\mu\mu} < 4$ GeV (i.e. a partially reconstructed B-meson mass). The second class consists of events in which the two muons originate from different beauty quarks of a $b\bar{b}$ pair. These can yield both like- and unlike-sign dimuon combinations, depending on whether the muon originates from the decay of the primary beauty quark, or from a secondary charm quark, and whether $B^0\overline{B^0}$ mixing has occurred. Such muons will predominantly be produced in different hemispheres, and tend to have a large dimuon mass.

An important background contribution arises from primary charm-pair production where both charm quarks decay into a muon. This yields unlike-sign muon pairs only, and the two muons are produced predominantly in opposite hemispheres. Since the charm background is too small to be measured directly from the dimuon data, it was normalised to the charm contribution from a ZEUS $D^* + \mu$ sample (Fig. 2 in [14]) which has a similar event topology and covers a similar though slightly more restricted kinematic range.

Other backgrounds yielding unlike-sign muon pairs include heavy quarkonium decays and Bethe-Heitler processes. In contrast to muons from semileptonic decays, muons from these sources are not directly accompanied by hadronic activity, thus giving an isolated muon signature.

Beauty production is the only source of genuine like-sign muon pairs. Background contributions to both like- and unlike-sign combinations include events in which either one or both muons are fake, i.e. originate from $K \to \mu$ or $\pi \to \mu$ decays, or misidentified hadrons. This background is referred to as light-flavour background. Studies [21] have shown that the charge of light-flavour fake muon pairs is almost uncorrelated, i.e. the contributions to the like- and unlike-sign dimuon distributions are almost equal, with only small and measureable corrections. The difference between the unlike- and like-sign distributions is thus essentially free from fake-muon background, without the need to simulate this background with Monte Carlo (MC) methods.

Once the other background contributions are known, the difference can therefore be used to measure the beauty contribution. This in turn can be used to measure the fake muon background by subtracting the beauty contribution from the total like-sign sample, and mirroring it onto the unlike-sign sample.

In this analysis, the beauty signal was hence extracted from the difference between the like and unlike-sign samples, while the like-sign sample was used to determine the contribution from fake-muon background to the unlike-sign sample.

Since one of the goals is the determination of the total beauty production cross section, events from the Deep Inelastic Scattering (DIS, photon virtuality $Q^2 > 1$ GeV^2) and photoproduction (PHP, $Q^2 < 1$ GeV^2) regimes were not explicitly separated.

4 Event Selection

4.1 Trigger Selection

The data were selected online by means of a three-level trigger system [15, 22] through a combination of four different trigger chains.

- A muon reaching the inner B/RMUON chambers and matched to a minimum ionizing energy deposit in the CAL or any muon reaching the outer B/RMUON chambers (muon chain) or
- a reconstructed D meson candidate (D^* chain [23], plus similar chains for other charm mesons) or
- two jets (dijet chain [10]) or
- a scattered-electron candidate in the CAL (DIS chain [11]).

For part of the data taking, the requirements on the DIS and dijet chains were loosened in the presence of any muon in the inner B/RMUON chambers. The non-muon triggers were used to gain in geometric acceptance for regions not covered by the B/RMUON chambers, and to evaluate the efficiency of the muon triggers.

Because of this redundancy, the trigger efficiency for dimuon events from beauty was high, $80 \pm 6\%$.

4.2 Muon Selection

Muons were reconstructed offline using a combination (“or”) of the following procedures:

- a muon track was found in the inner B/RMUON chambers. Then a match in position and angle to a CTD track was required. In the bottom region, where no inner chambers are present, the outer chambers were used instead. If a match was found to both inner and outer chambers, a momentum matching criterion was added;
- a muon track was found in the FMUON chambers. Generally a match in position and angle to a CTD track was required. For high quality candidates outside the CTD acceptance the match to a CTD track was replaced by a match to the primary vertex. The muon momentum was obtained from a combined fit of the CTD and FMUON momentum information;
- a muon track or localised energy deposit was found in the BAC, and matched to a CTD track, from which the muon momentum was obtained. In the forward region of the detector, a MIP in the calorimeter was required in addition in order to reduce background related to the proton beam or to the punchthrough of high energy hadrons.

Most muons are detectable by more than one of these algorithms. The overall selection yields a detection efficiency of about 80% for high momentum muons.

In the barrel region, the requirement that the muons reach at least the inner muon chambers implies a transverse momentum cut of

$$p_T^\mu > 1.5\,\mathrm{GeV} \tag{1}$$

In order to have uniform kinematic acceptance and acceptable background, this cut was also applied in general in the rear and forward regions. For high quality muons seen by more than one muon detector and/or confirmed by a MIP in the CAL, this cut was lowered to

$$p_T^\mu > 0.75\,\mathrm{GeV} \tag{2}$$

in order to gain acceptance mainly in the forward and rear regions. This is important to cover the maximum possible phase space for the intended total cross section measurement.

No explicit cut on the muon angle was applied. The angular coverage of the muon chambers, BAC and CTD yield significant and continous muon acceptance in the approximate pseudorapidity region

$$-2.2 \lesssim \eta^\mu \lesssim 2.5\ . \tag{3}$$

At least two such muon candidates were required per event.

To suppress events with ambiguous matches between the tracks and the muon chamber segments as well as light-flavour background (e.g. $\rho \to \mu\mu$ decays etc.), a lower dimuon invariant mass cut of

$$m^{\mu\mu} > 1.5\ \ \mathrm{GeV} \tag{4}$$

was applied. This implicitly ensures a minimum opening angle between the two muon candidates.

Background with a very forward and a very backward muon candidate, a topology not favoured for the beauty sample to be measured, was removed by a cut on the difference in pseudorapidity of the two muon candidates of

$$|\eta^{\mu_1} - \eta^{\mu_2}| < 3.0. \tag{5}$$

Badly measured muon candidates (predominantly from light-flavour backgrounds) were suppressed using the imbalance between the transverse momenta of the muons

$$(|p_{\rm T}^{\mu_1} - p_{\rm T}^{\mu_2}|)/(p_{\rm T}^{\mu_1} + p_{\rm T}^{\mu_2}) < 0.7. \tag{6}$$

Cosmic ray muons were suppressed by discarding events with back-to-back muon candidates and events in which the average calorimeter timing differs more than 10 ns from the nominal collision time. Large cosmic showers were suppressed using the BAC total energy and number of BAC muon segments.

4.3 General Selection

The large mass of a $b\bar{b}$ pair, at least ~ 10 GeV, usually leads to a significant amount of energy deposited in the more central parts of the detector. To suppress backgrounds from light flavour events and charm, a cut

$$E_{\rm T} \geq 8 \ \text{GeV} \tag{7}$$

was applied, with

$$E_{\rm T} = \begin{cases} E_{\rm T}^{\rm cal} - E_{\rm T}^{\rm cal}|_{\text{in } 10^\circ \text{ forward cone}} & \text{no scattered electron} \\ E_{\rm T}^{\rm cal} - E_{\rm T}^{\rm cal}|_{\text{in } 10^\circ \text{ forward cone}} - E_{\rm T}{}^{electron} & \text{with scattered electron.} \end{cases} \tag{8}$$

defined as the transverse energy reconstructed in the CAL ($E_{\rm T}^{\rm cal}$) outside a cone of 10° around the proton beam direction (to remove proton remnant effects), excluding the scattered electron (if detected). The detection criteria for the scattered electron were the same as in [14].

An additional cut with a similar influence was applied on the fraction of the total transverse energy carried by the muon pair

$$0.1 < (p_T^{\mu_1} + p_T^{\mu_2})/E_{\rm T} < \begin{cases} 0.5 & \text{for } m^{\mu\mu} < 4 \ \text{GeV} \\ 0.7 & \text{for } m^{\mu\mu} \geq 4 \ \text{GeV} \end{cases} \tag{9}$$

This E_{T}-fraction cut removes events with very high (background) or low (not beauty) hadronic activity in addition to the muons.

Finally cleaning cuts [21] are imposed at the tracking level, requiring a well defined event vertex.

With all these cuts, a sample of 4039 dimuon events was obtained.

5 Backgrounds and event simulation

In order to measure the beauty cross section several contributions to the selected data sample needed to be evaluated:

- the signal from beauty decays;
- the contribution from charm decays, which is a background to the beauty signal;
- the contributions from quarkonium states not originating from B hadron decays (J/ψ, ψ', Υ, ...), which are again treated as background;
- the background from Bethe-Heitler muon pair production;
- the background from fake or non-prompt muons.

Monte Carlo (MC) simulations of beauty and charm production were performed using the generators Pythia [24] (for events with $Q^2 < 1$ GeV^2) and Rapgap [25] (for $Q^2 > 1$ GeV^2). These simulations include the direct photon-gluon-fusion process ($\gamma g \to Q\bar{Q}$, $Q = b, c$), flavour excitation in the resolved photon and proton (e.g. $Qg \to Qg$, $\gamma Q \to Qg$), and hadron-like resolved photon processes (e.g. $gg \to Q\bar{Q}$). Gluon splitting into heavy flavours ($g \to Q\bar{Q}$) in the initial or final states of light-quark events was not included in the simulations; this contribution is, however, expected to be small.

Inelastic quarkonium production was simulated using Herwig [26], while elastic quarkonia and Bethe-Heitler processes, most of which are eliminated by the general selection cuts described above, were produced using a variety of generators including GRAPE [27].

For all generated events, the ZEUS detector response was simulated in detail using a programme based on GEANT 3.21 [28]. The detector simulation for the beauty and charm events includes the simulation of both real and fake muons.

Fake muons can be produced by hadron showers leaking from the back of the calorimeter or by charged hadrons traversing the entire calorimeter without interaction. In addition, low-momentum muons can originate from in-flight decays of pions and kaons. Finally, tracks reconstructed in the central tracker may be wrongly associated to a signal from a real muon in the muon chambers. A study [29] based on pions from K^0 decays, protons from Λ decays, and kaons from ϕ and D^* decays, showed that the detector simulation reproduced these backgrounds reasonably well.

Corrections for imperfections in the simulation of the real MC muon reconstruction efficiency were applied. The MC correction factors were determined from the data based on an independent set of isolated J/ψ and Bethe-Heitler events.

Backgrounds from fake muons in light flavour events were not simulated. They were estimated from the data using the procedure described in section 3.

6 Signal extraction

Dimuon mass and charge separation

As motivated earlier, events were separated by the muon charges into like- and unlike-sign dimuon samples.

To differentiate between muon pairs from the cascade decay of *the same* b quark and those from *different* b quarks, the distributions were further separated depending on the dimuon invariant mass. Events were plotted separately for subsamples of low-mass dimuons with $m^{\mu\mu} < 4$ GeV, enriched in muons from the same b quark, and of high-mass dimuons with $m^{\mu\mu} > 4$ GeV, containing dimuons originating from the decay of different b quarks.

The dominating signal and background contributions to the 4 subsamples are summarised in Table 1.

The resulting dimuon mass distributions for the low and high mass, like and unlike-sign subsamples are shown in Fig. 1. All predicted contributions were normalized to the data according to the procedure described in the next sections. The high mass region is already strongly beauty enriched, while the low mass region exhibits a significant contribution from J/ψ production not originating from b decays.

Dimuon isolation cuts

To reduce this contribution, as well as corresponding contributions from ψ',Υ and Bethe-Heitler processes, a non-isolation requirement was applied, using the fact that muons from semileptonic decays are accompanied by hadrons from the same decay. The energy flow from these hadrons was reconstructed using a combination of track and calorimeter information that optimises its resolution [30]. The selected tracks and clusters are referred to as energy flow objects (EFOs). First, the difference in azimuth angle and pseudorapity, $\Delta\phi$ and $\Delta\eta$, was calculated between each EFO and each muon candidate in the event. The total transverse energy $I_{1,2}$ deposited in a cone of $\Delta R = \sqrt{\Delta\phi^2 + \Delta\eta^2} < 1$ around each muon flight direction was calculated by summing over all relevant EFO's, excluding the other muon. Since usually either both or none of the muons arise from semileptonic decays, the quadratic sum $I^{\mu\mu} = \sqrt{I_1^2 + I_2^2}$ of the two energy sums was found to yield the best sensitivity. It was required to exceed 250 MeV, safely above the noise level of the CAL.

In inelastic quarkonium and Bethe-Heitler events, hadrons from e.g. the proton remnant can accidentally end up in the isolation cone, and exceeed this cut. For events in the J/ψ and ψ' mass peaks, where this background is largest, the cut was therefore raised to 2 GeV.

In summary, dimuons fulfilling the relation

$$I^{\mu\mu} \geq \begin{cases} 2.0 \ \text{GeV} & \text{for } m^{\mu\mu} \in [2.9,\ 3.25] \text{ or } m^{\mu\mu} \in [3.6,\ 3.75] \\ 0.25 \ \text{GeV} & \text{otherwise} \end{cases} \tag{10}$$

are called nonisolated. All other dimuon events are part of the isolated background subsample.

Figure 2 shows the muon p_T and η distribution for nonisolated unlike-sign dimuon pairs, combining the low and high mass samples. The remaining contribution from J/ψ, Bethe Heitler (BH), etc. processes was normalised such that the corresponding isolated distributions, in which these processes dominate, are reproduced. The charm contribution is small and was normalised to the charm signal in the $D^* + \mu$ sample of [14] as outlined in section 3. The procedure to extract the beauty signal and light flavour background contributions is described in the next section.

Signal extraction

The beauty contribution to the total event sample in both like- and unlike-sign dimuon events was determined by exploiting the charge symmetry of the light-flavour backgrounds. As there is an (almost, see below) equal contribution from this background in the like- and unlike-sign dimuon sample,

$$N^{\mathrm{u}}_{\mathrm{bg}} = N^{\mathrm{l}}_{\mathrm{bg}}, \tag{11}$$

the difference between these samples is essentially free from light-flavour background. From this difference sample the remaining backgrounds (charm, J/ψ, ψ' and BH) were subtracted using the normalised background-MC samples. The remainder is the difference of unlike- and like-sign dimuon events from beauty. The extrapolation to the sum of like- and unlike-sign dimuon events is done using the beauty MC:

$$N_{b\bar{b}\to\mu\mu} = \left(N^{\mathrm{u}}_{\mathrm{data}} - N^{\mathrm{l}}_{\mathrm{data}} - \left(N_{\mathrm{charm}} + N_{J/\psi} + N_{\mathrm{BH}} + ...\right)\right) \times \left(\frac{N^{\mathrm{u}}_{b\bar{b}} + N^{\mathrm{l}}_{b\bar{b}}}{N^{\mathrm{u}}_{b\bar{b}} - N^{\mathrm{l}}_{b\bar{b}}}\right)^{\mathrm{MC}} \tag{12}$$

Events from unlike-sign background sources which have falsely been reconstructed as like-sign dimuon events are included both in the light-flavour background estimation and in the MC samples. To avoid double counting, this (very small) contribution is subtracted from the MC samples. Falsely reconstructed beauty MC muons are considered as signal (if they lead to an excess of unlike sign events).

Corrections for background charge correlations

A dedicated fake muon background study [21] revealed a small residual excess of unlike-sign over like-sign background. This excess amounted to 2% difference in the high mass and 6% difference in the low-mass dimuon sample, thus

$$N_{\mathrm{bg}}^{\mathrm{u}} = \alpha_{\mathrm{corr}} \cdot N_{\mathrm{bg}}^{\mathrm{l}}, \tag{13}$$

where the correction factor α_{corr} is

$$\alpha_{\mathrm{corr}} = \begin{cases} 1.02 & \text{for the high mass } (m^{\mu\mu} > 4 \text{ GeV) signal sample} \\ 1.06 & \text{for the low mass } (m^{\mu\mu} < 4 \text{ GeV) signal sample.} \end{cases} \tag{14}$$

To account for this background charge asymmetry, the beauty fraction was determined using a corrected version of (12)

$$N_{b\bar{b}\to\mu\mu} = \left(N_{\mathrm{data}}^{\mathrm{u}} - \alpha_{\mathrm{corr}} \cdot N_{\mathrm{data}}^{\mathrm{l}} - \left(N_{\mathrm{charm}} + N_{J/\psi} + N_{\mathrm{BH}} + ...\right)\right) \times \left(\frac{N_{b\bar{b}}^{\mathrm{u}} + N_{b\bar{b}}^{\mathrm{l}}}{N_{b\bar{b}}^{\mathrm{u}} - \alpha_{\mathrm{corr}} \cdot N_{b\bar{b}}^{\mathrm{l}}}\right)^{\mathrm{MC}}. \tag{15}$$

A total beauty contribution to the nonisolated sample of about 1900 events was obtained with a purity of about 50%.

7 Theoretical predictions and uncertainties

The Monte Carlo programs described earlier, based on leading order matrix elements with the addition of parton showers to obtain higher order topologies, were used for acceptance correction purposes. They are expected to describe the shapes of differential distributions, but not necessarily their normalisation. For quantitative comparisons with QCD, next-to-leading order (NLO) predictions are used.

Calculations in which b quarks are treated as massless particles [31] are not applicable in the kinematic range relevant here, while calculations based on alternative parton evolution schemes [32] do not yet exist with full NLO implementation. Fixed order calculations with massive b quarks should yield accurate predictions. Different types of such predictions were evaluated.

The FMNR program [1] evaluates cross sections for next-to-leading-order beauty production in γp collisions (photoproduction) in the fixed-order massive mode, for both pointlike and hadron-like photon coupling to the heavy quarks. The parton density functions used were CTEQ5M [33] for the proton, and GRV-G-HO [34] for the photon. The renormalisation and factorisation scales μ were chosen to be equal and parametrised by $\mu_0 = \sqrt{p_T^2 + m_b^2}$, where p_T is the average transverse momentum of the two emerging b quarks, and $m_b = 4.75$ GeV is their invariant mass. An estimate of the theoretical uncertainty was obtained by simultaneously varying $4.5 < m_b < 5.0$ GeV and $\mu_0/2 < \mu < 2\mu_0$ such that the uncertainty was maximised. Typical uncertainties resulting from this procedure (e.g. for the $b\bar{b}$ total cross section) are +40% and -25%. Variations of the parton densities led to uncertainties which were much smaller than the uncertainties related to mass and scale variations. They were therefore neglected.

Predictions at the level of visible $\mu\mu$ final states are needed in addition to those at parton level. The FMNR program provides a framework to fragment b quarks into B hadrons, and simulate the decay of these hadrons by interfacing them to appropriately chosen decay spectra. However, decays to complicated final states, such as two muons from the same B hadron with cuts on both particles, cannot be easily implemented in this scheme. A straightforward interface of the parton-level events produced by FMNR to MC-like fragmentation and decay chains is also not practical, since these events have positive and negative weights spanning more than 8 orders of magnitude, making such an approach extremely inefficient.

These difficulties were overcome in a two-step process. In the first step, two or more FMNR parton level events with large positive and negative weights and similar topology (similar momenta and angles of the emanating b quarks) are iteratively combined into events with much smaller (but still positive and negative) weights by averaging the parton momentum vectors [35]. Events are considered to have similar topology if the difference in transverse momentum, rapidity and azimuthal angle of the b quarks are less than user cut values (1 GeV, 0.2, 0.3 rad) which reflect the detector resolution. The iterations are stopped when the weights are smaller than a predefined threshold. It was explicitly checked that this procedure preserves the NLO accuracy for the relevant cross sections at parton level (e.g. b quark p_T and angular distributions). Furthermore, events with small weights were selected with a probability proportional to their weight (sampling approach). In this way, the weight range was reduced to about two orders of magnitude.

In the second step, these parton level events were interfaced to the Pythia/Jetset [36] fragmentation and decay chain, making use of the full decay tables and decay kinematics implemented in Pythia 6.2. Therefore, non-dominant arbitrarily complicated decays, such as $B \to D\bar{D}$ followed by semileptonic decays of both D mesons, or muons through intermediate J/ψ or τ states, were automatically included. The initial state partons were allowed to have intrinsic k_T (typically $\sim$ 300 MeV) as implemented in PYTHIA. This has a negligible effect on the resulting cross sections ($\sim 1\%$). Parton showering was not allowed in order to avoid double counting of higher order contributions[3].

Fragmentation of b quarks close to production threshold is nontrivial. The details of the threshold treatment were found to be much more important than the choice of a particular fragmentation function. The Peterson formula [38] with $\epsilon = 0.0035$ was used. Three approaches were considered:

- independent fragmentation as implemented in PYTHIA [36]. The use of this quite old model was motivated by the fact that FMNR does not provide colour connections on an event-to-event basis;
- fragmentation in the Lund string model [39], again as implemented in PYTHIA. For this purpose, reasonable colour connections were assigned to each event;
- the independent fragmentation scheme provided within the FMNR framework, rescaling the B hadron momentum to a fraction of the b-quark momentum according to the Peterson formula. This avoids threshold corrections due to the need for simultaneous momentum and energy conservation, but is a somewhat crude approximation at threshold.

The second option was used for all central predictions. The first option was used to obtain the lower systematic error (typically -5%). The third option could not be applied directly, since it does not provide cross-section predictions for correlated final states from the same b quark as needed here. Instead, it was applied to a cross section in which the final state correlations originate from different b quarks only, which is more easily calculable in this scheme. The results were used to evaluate a generic upper systematic error on the fragmentation procedure close to b production threshold of +15%. The effect of a variation of the Peterson parameter ϵ in the range 0.0023 to 0.0045 was found to yield uncertainties which were much smaller than the uncertainties due to the different fragmentation procedures. It was therefore neglected.

The branching ratios were empirically corrected to correspond to those obtained from the Particle Data Group (PDG) [40], as listed in Table 2. This yields dimuon cross section uncertainties of typically $\pm 6\%$.

In principle FMNR predictions are valid only for the photoproduction regime. The Weizsäcker-Williams (WW) approximation with an effective $Q^2_{\rm max}$ cutoff of 25 GeV^2

[3] The MC@NLO approach [37], which *does* allow the combination of NLO matrix elements with parton showers, is not yet available for ep interactions.

($\sim m_b^2$) [41] was used to include the ∼15% DIS contribution to the combined cross section.

Alternatively, the DIS part can be calculated using the NLO predictions from HVQDIS [2]. Only point-like contributions are included in this prediction. The parton density function used was CTEQ5F4 [33]. The renormalisation and factorisation scales μ were chosen to be equal and parametrised by $\mu_0 = \sqrt{Q^2 + m_b^2}$. The mass and scales were varied as for FMNR. A scheme for the calculation of visible cross sections for correlated final states, corresponding to the FMNR⊗PYTHIA interface described above, was not available. Therefore, DIS cross-section comparisons are limited to parton level, and the DIS contribution to the inclusive cross sections is included in the FMNR⊗PYTHIA predictions via the WW approximation.

8 Systematic uncertainties

The main systematic uncertainties are described below, in approximate order of importance. Numbers in parentheses are quoted for the visible cross section used to derive the total cross section. Bin-by-bin errors have been evaluated for the differential distributions where possible and appropriate. They are mostly similar to the ones derived for the inclusive case. Additional errors for the extrapolation to quark level are discussed later.

- **Muon efficiency correction.** The muon acceptance, including the efficiency of the muon chambers, of the reconstruction, and of the MUON-CTD matching, is known to about 7% from a study based on an independent muon sample, and from the variance of the cross section when information from different muon detectors is used independently [21]. It is assumed to be fully correlated between the two muons (±15%).
- **Normalisation of charm background.** The transfer of the normalisation of the charm contribution from the $D^*\mu$ analysis [14] to this analysis involves several uncertainties. The statistical error of the fit of the charm contribution (10%), the inclusive branching ratio $c \to \mu$ (10%), the acceptance uncertainty due to charm fragmentation and decay spectra (10%), the fragmentation fraction $c \to D^{*\pm}$ (6%), the branching ratio $D^{*\pm} \to K\pi\pi$ (3%), and the use of all muon detectors (this analysis) versus the use of the barrel and rear muon chambers only [14] (10%). The influence of the correlation between the fitted beauty and charm fractions in [14] was found to be negligible. This yielded a combined uncertainty on the normalization of the charm contribution of 21%, which was varied accordingly (±12%).
- **Normalisation of the BH, J/ψ, etc. backgrounds.** The normalisation of the residual backgrounds from Bethe-Heitler, charmonium, and Υ production (non-isolated tails) were varied by ±50% (±10%).

- **b spectral shape uncertainty and $b\bar{b}$ correlations.** It was checked that the b-quark spectra from PYTHIA and RAPGAP agree well with the corresponding spectra from the NLO predictions described below [29]. To estimate the effect of variations of this shape, and of effects of variations of the $b\bar{b}$ correlations for different topologies on the acceptance, the acceptance was evaluated using the PYTHIA direct contribution only, or doubling the non-direct contributions (+4%/-12%).
- **MC model uncertainties.** The sensitivity to other MC model uncertainties (fragmentation, decay etc.) was estimated for both the signal MC and the charm background MC (+10%/-11%).
- **$B^0\bar{B}^0$ oscillations.** The $B^0\bar{B}^0$ oscillation parameter was varied by 8% ($\pm$4%).
- **Trigger efficiency.** The uncertainty on the trigger efficiency was estimated by comparing the efficiencies for muon and non-muon triggers in data and MC ($\pm$8%).
- **Other uncertainties.** Other uncertainties include the variation of the like/unlike sign ratio for the light flavour background by 3% ($\pm$3%), the variation of the isolation cuts by 500 MeV ($\pm$2%), the variation of the E_T cut by 3% (energy scale, $\pm$2%), the variation of the p_T^μ cuts by 0.3% (magnetic field uncertainty, < 1%).

The total systematic uncertainty was obtained by adding the above contributions in quadrature. A 2% overall normalization uncertainty associated with the luminosity measurement was not included.

9 Total $b\bar{b}$ cross section

As a first step towards the extraction of a total cross section for $b\bar{b}$ production, a visible cross section was extracted for the maximum possible muon phase space region allowed by the preselection and the detector acceptance. Using the criterion that the muon detection efficiency should be at least about 30% per muon, this phase space was obtained to be:

- $-2.2 < \eta < 2.5$ for both muons (effective rapidity acceptance);
- $p_T > 1.5$ GeV for one of the two muons (standard p_T^μ cut);
- $p_T > 0.75$ GeV for the other muon (low p_T^μ cut), as well as $p > 1.8$ GeV for $\eta < 0.6$, or ($p > 2.5$ GeV or $p_T > 1.5$ GeV) for $\eta > 0.6$ (effective detector acceptance).

Only one pair of muons is considered per event. If there is more than one, muons directly originating from B decays are preferred over muons from secondary chain decays (e.g. via charm). Correcting for muon acceptance, a visible cross section for dimuon production from beauty decays in this phase space

$$\sigma_{\mathrm{vis}}(ep \to b\bar{b}X \to \mu\mu X') = 63 \pm 7(\mathrm{stat.})^{+20}_{-18}(\mathrm{syst.})\ \mathrm{pb} \qquad (16)$$

was obtained. This cross section includes muons from direct b hadron decays, and indirect decays via intermediate charm hadrons or τ leptons. The two muons can either originate from the same b quark, or from different quarks of the $b\bar{b}$ pair. Muonic decays of kaons, pions or other light hadrons were not included. Events containing more than two muons were counted only once.

The measured cross section is larger than, but compatible with, the FMNR$\otimes$PYTHIA NLO prediction

$$\sigma_{vis,NLO}(ep \to eb\bar{b}X \to e\mu\mu X) = 30^{+9}_{-6}(\mathrm{NLO})^{+5}_{-3}(\mathrm{frag.} \oplus \mathrm{br.})\ \mathrm{pb}, \quad (17)$$

where the first error refers to the uncertainties of the FMNR parton level calculation, and the second error refers to the uncertainties related to fragmentation and decay.

The low muon p_T threshold gives sensitivity to b-quark production down to $p_T^b = 0$ (Fig. 3). In combination with the large pseudorapidity coverage, this allows the extraction of the total cross section for beauty production. The b quark p_T and rapidity spectra predicted by the PYTHIA and RAPGAP generators were found to agree with those from FMNR and HVQDIS to within 15% [29]. They can therefore be used for an extrapolation to the total cross section.

The probability of a $b\bar{b}$ pair to yield a muon pair in the visible kinematic range (0.38% on average) is quite small. However, it is almost entirely dominated by quantities measured with good precision at e^+e^- colliders.

The effective branching fraction of a $b\bar{b}$ pair into at least two muons is 6.3% [24, 40]. Both the b fragmentation functions and the b hadron $\to$ μX decay spectra are well measured [40] and yield an average acceptance for the visible range of 6%. These two factors taken together yield the quoted acceptance of 0.38%. Furthermore, the value of the latter varies by only a factor 3 (from 3% to 9%) in 90% of the $b\bar{b}$ phase space, delimited by $0 < p_{Tb}^{\max} < 10$ GeV or $|\zeta_b|^{\min} < 2$. Here $p_{Tb}^{\max}$ denotes the maximum p_T of the two b quarks after parton showering, and $|\zeta_b|^{\min}$ the minimum of the modulus of the rapidity (not pseudorapidity) of the two quarks. At larger p_T^b the acceptance rises, but the fraction of events is small. In rapidity, only 10% of the total beauty contribution in the region $\zeta_b^{\min} > 2$ remains unmeasured. This uniformity of acceptance means that the dependence on details of the simulation of the $b\bar{b}$ topology is rather weak, and that the extrapolation to unmeasured regions is small.

In order to agree with the data, the normalisation of the PYTHIA + RAPGAP MC prediction for the beauty contribution had to be scaled up by a factor 2.06. Scaling the total PYTHIA and RAPGAP cross sections accordingly, the total cross section for $b\bar{b}$ pair production in ep collisions at HERA for $\sqrt{s} = 318$ GeV was obtained to be

$$\sigma_{\mathrm{tot}}(ep \to b\bar{b}X) = 16.1 \pm 1.8(\mathrm{stat.})^{+5.3}_{-4.8}(\mathrm{syst.})\ \mathrm{nb}, \quad (18)$$

where the first uncertainty is statistical, and the second systematic. In addition to the errors described in section 8, this includes an error of 5% from the uncertainties of the spectral shape mentioned above, and an error of 6% from the variation of the branching ratios, added in quadrature.

The total cross section predicted by next-to-leading order (NLO) QCD calculations was obtained in the massive approach by adding the predictions from FMNR [1] and HVQDIS [2] for $Q^2 <,> 1$ GeV^2, respectively. The resulting cross section for $\sqrt{s} = 318$ GeV

$$\sigma_{\rm tot}^{\rm NLO}(ep \to b\bar{b}X) = 6.8^{+3.0}_{-1.7}\ \rm nb \tag{19}$$

is a factor 2.4 lower than the measured value, although still compatible within the large uncertainties. The corresponding cross section from FMNR only using the Weizsäcker-Williams approximation to estimate the DIS contribution amounts to

$$\sigma_{\rm tot}^{\rm WW}(ep \to b\bar{b}X) = 7.0^{+3.0}_{-1.7}\ \rm nb, \tag{20}$$

in agreement with the more exact FMNR+HVQDIS calculation.

The fact that the comparisons between data and theory yield the same ratio at visible (equations (16)/(17))

$$R_{vis}^{\rm data/NLO} = 2.1^{+0.8}_{-1.0} \tag{21}$$

and quark level (equations (18)/(20))

$$R_{b}^{\rm data/NLO} = 2.3^{+1.0}_{-1.2} \tag{22}$$

confirms the validity of the extrapolation procedure used.

10 Differential cross sections and $b\bar{b}$ correlations

The same method was used to derive differential cross sections. To simplify the measurements and avoid complicated η,p_T correlations, a unique p_T cut of $p_T^\mu > 1.5$ GeV was required for both muons at reconstruction and true level. All other cuts remain the same as before. This retained about 2/3 of the originally selected sample. The backgrounds were again normalized as described in section 6. The signal-extraction procedure was the same as for the inclusive visible cross section, except that it is now applied bin-by-bin. Bin-dependent systematic uncertainties were calculated wherever possible. The resulting cross sections for the differential p_T^μ and η^μ spectra are shown in Figs. 4 and 5. Very good agreement is observed with the Pythia+Rapgap predictions scaled by a factor 1.95. This factor does not differ significantly from that for the inclusive selection. Apart from the normalisation, the leading order plus parton shower (LO+PS) approach yields a good description of the corresponding physics processes within the entire accessible phase space. This confirms the applicability of these MC models for acceptance calculations.

A comparison of the measured cross sections to the absolute FMNR⊗Pythia NLO predictions is also shown in Figs. 4 and 5. Again, good agreement in shape is observed, with a tendency to underestimate the data normalisation consistent with the observations from the total cross section. This measurement has a lower p_T threshold and wider η range than previous measurements. A potential trend for increasing data/theory deviations towards low p_T and/or high η, suggested by some of these previous measurements [9, 11], is not supported.

To have a more detailed look at the correlations between the two b-quarks, the reconstructed dimuon mass range was restricted to $m^{\mu\mu} > 3.25$ GeV. This reduced the contribution of dimuons from the same quark to an almost negligible level. The corresponding data distribution for $\Delta\phi$ between the two muons is shown in Fig. 6. Consequently, at true level, muons were now required to originate from different b-quarks. This results in the differential cross section shown in Fig. 7. The distribution is reasonably described by the FMNR⊗Pythia NLO predictions within the large errors resulting from the subtraction method (15). The leading order contribution alone, which is also shown, reproduces the measured distribution less well. Although the difference in shape is not dramatic, due to the smearing from the semileptonic decays, this confirms the importance of the contributions from higher order processes.

11 Comparison to other measurements

Figure 8 shows a comparison of the measured total cross section to the slightly less inclusive cross sections from the $D^* + \mu$ final state obtained by ZEUS in earlier measurements [14]. These measurements, as well as similar measurements by H1 [13] show the same trend of being larger than the corresponding QCD predictions.

In order to compare to other previous ZEUS results [10, 11], expressed in terms of parton level cross sections differential in p_T^b, similar cross sections were also derived here.

The first step was the derivation of visible cross sections for B hadrons in different p_T ranges. For this purpose, the data sample used for the measurement of the total beauty cross section was split into two subsamples, with $m^{\mu\mu} > 3.25$ GeV and $m^{\mu\mu} < 3.25$ GeV. As motivated in the previous section, the $m^{\mu\mu} > 3.25$ sample is dominated by muons from different b quarks, with correlations between the two quarks which are reasonably understood. Thus, two distinct B hadrons have been measured in each event. In order to estimate the transverse momenta of these B hadrons, the quantitity

$$E_T^{vis} = p_T^{\mu} + I^{\mu} \tag{23}$$

is built independently for each muon, where I^{μ} is the cone transverse energy described in section 6. This variable is found to be strongly correlated to the parent B hadron transverse momentum at high p_T, where the additional energy from b quark fragmentation to the B hadron compensates the loss due to the unreconstructed neutrino from the semileptonic decay. At $p_T \lesssim m_b$, this correlation is diluted by the effect of the B hadron mass and the corresponding decay kinematics.

Fig. 9(a) shows the expected B hadron p_T spectra for 3 bins in E_T^{vis}, $0 < E_T^{vis} < 5$ GeV, $5 < E_T^{vis} < 10$ GeV, and $10 < E_T^{vis} < 40$ GeV. Reasonably distinct B hadron p_T regions are probed. The corresponding cross sections are shown in Fig. 10(a).

A similar procedure is applied to the subsample with $m^{\mu\mu} < 3.25$ GeV. In this sample, the muons originate mainly from the same b quark, therefore only one B hadron has been measured. Due to branching ratios and decay kinematics, the cross section is smaller, but the unlike sign/like sign ratio is much more favourable (no like sign muon pairs from same b). Therefore, the significance of the measurement is comparable to that from the high mass region. Furthermore, the subtraction method eliminates a large part of the residual contribution of muons from different b quarks to this region, making it almost completely insensitive to $b\bar{b}$ correlations.

The E_T^{vis} variable is redefined to

$$E_T^{vis} = p_T^{\mu\mu} + I^{\mu}_{\mathrm{high}} \tag{24}$$

where $p_T^{\mu\mu}$ is the transverse momentum of the dimuon system added vectorially, and I^{μ}_{high} is the isolation of the higher p_T muon only, to avoid double counting. The correlations to the B hadron p_T are similar to the high mass case (Fig. 9(b)). The resulting visible B hadron cross sections are shown in Fig. 10(b).

For both subsamples, reasonable agreement is found with the FMNR$\otimes$Pythia predictions, consistent with the conclusions obtained earlier.

The second step is to extrapolate these cross sections to b quark level, and to restrict them to photoproduction for the comparison with previous measurements. Each of the B hadron visible cross sections is translated into a differential cross section $\frac{d\sigma}{dp_T^b}$ in the pseudorapidity range $|\eta_b| < 2$ [10][4] with photon virtuality $Q^2 < 1$ GeV and inelasticity $0.2 < y < 0.8$, using the FMNR$\otimes$Pythia predictions. Each cross section is quoted at the

[4] Figure 7 and Table 6 of [10] report measured cross sections and theory for b-quark rapidity smaller than one rather than for $|\eta_b| < 2$ by mistake.

mean p_T^b value for events satisfying the cuts for the corresponding E_T^{vis} bin. The results are shown in Fig. 11.

As the cross sections derived from the low and high mass subsamples (same and different b quarks) agree with each other, they can be combined to a single cross section for each E_T^{vis} bin. The maximum possible correlation of the systematic errors is assumed for this combination.

The resulting combined cross sections are compared to theory and previous measurements in Fig. 12. They are consistent with these previous measurements, and extend the measured range to low p_T^b.

12 Conclusions

The total cross section for beauty production in ep collisions at HERA (mainly photoproduction, but including a DIS contribution of about 15%) has been measured using an analysis technique based on the detection of two muons, mainly from semileptonic beauty decay. The almost complete phase space coverage and only weak dependence on details of the $b\bar{b}$ event topology allows a reliable extraction of the total beauty production cross section, with small extrapolation, and a direct comparison to NLO QCD predictions. These predictions are lower than the observed cross sections, but compatible within the uncertainties. Differential cross sections in p_T^μ, η^μ, and $\Delta\phi^{\mu\mu}$ were also obtained, and found in very good agreement with the shapes predicted by Monte Carlo models incorporating leading order matrix elements followed by parton showers. NLO QCD predictions agree in shape with both the data and the LO+PS predictions, but are again somewhat lower than the data, in agreement with the observation from the total cross section. No particular trend in p_T or rapidity is observed. Measurements of cross sections for muon pairs from the same or from different B hadrons yield similar and compatible results. A comparison with previous measurements through the extrapolation to differential cross sections at b quark level shows reasonable agreement, and extends these measurements down to very low p_T.

Acknowledgements

We thank the DESY Directorate for their strong support and encouragement. The remarkable achievements of the HERA machine group were essential for the successful completion of this work and are greatly appreciated. We are grateful for the support of the DESY computing and network services. The design, construction and installation of the ZEUS detector have been made possible owing to the ingenuity and effort of many people who are not listed as authors. It is also a pleasure to thank S. Frixione for help with the theoretical predictions.

References

[1] S. Frixione et al., Nucl. Phys. **B 412**, 225 (1994);
S. Frixione, P. Nason and G. Ridolfi, Nucl. Phys. **B454** (1995);
M. Cacciari, S. Frixione and P. Nason, JHEP **0103**, 006 (2001).

[2] B.W. Harris and J. Smith, Nucl. Phys. **B 452**, 109 (1995);
B. W. Harris and J. Smith, Phys. Lett. **B 353**, 535 (1995). Erratum-ibid **B 359** (1995) 423;
B.W. Harris and J. Smith, Phys. Rev. **D 57**, 2806 (1998).

[3] UA1 Coll., C. Albajar et al., Phys. Lett. **B 186**, 237 (1987);
UA1 Coll., C. Albajar et al., Phys. Lett. **B 256**, 121 (1991). Erratum-ibid. **B 262**, 497 (1991);
UA1 Coll., C. Albajar et al., Z. Phys. **C 61**, 41 (1994).

[4] CDF Coll., F. Abe et al., Phys. Rev. Lett. **71**, 500 (1993);
CDF Coll., F. Abe et al., Phys. Rev. Lett. **71**, 2396 (1993);
CDF Coll., F. Abe et al., Phys. Rev. Lett. **75**, 1451 (1995);
CDF Coll., F. Abe et al., Phys. Rev. **D 53**, 1051 (1996);
CDF Coll., D. Acosta et al., Phys. Rev. **D 65**, 052005 (2002);
CDF Coll., D. Acosta et al., Phys. Rev. **D 71**, 032001 (2005);
DØ Coll., S. Abachi et al., Phys. Rev. Lett. **74**, 3548 (1995);
DØ Coll., B. Abbott et al., Phys. Lett. **B 487**, 264 (2000);
DØ Coll., B. Abbott et al., Phys. Rev. Lett. **84**, 5478 (2000);
DØ Coll., B. Abbott et al., Phys. Rev. Lett. **85**, 5068 (2000).

[5] L3 Coll., M. Acciarri et al., Phys. Lett. **B 503**, 10 (2001);
L3 Coll., P. Achard et al., Phys. Lett. **B 619**, 71 (2005).

[6] WA78 Coll., M. Catanesi et al., Phys. Lett. **B 202**, 453 (1988);
E672/E706 Coll., R. Jesik et al., Phys. Rev. Lett. **74**, 495 (1995).

[7] E771 Coll., T. Alexopoulos et al., Phys. Rev. Lett. **82**, 41 (1999);
D.M. Jansen et al., Phys. Rev. Lett. **74**, 3118 (1995);
HERA–B Coll., I. Abt et al., Eur. Phys. J. **C 26**, 345 (2003).

[8] H1 Coll., C. Adloff et al., Phys. Lett. **B 467**, 156 (1999);
ZEUS Coll., J. Breitweg et al., Eur. Phys. J. **C 18**, 625 (2001).

[9] H1 Coll., A. Aktas et al., Eur. Phys. J. **C 41**, 453 (2005).

[10] ZEUS Coll., S. Chekanov et al., Phys. Rev. **D 70**, 12008 (2004).

[11] ZEUS Coll., S. Chekanov et al., Phys. Lett. **B 599**, 173 (2004).

[12] H1 Coll., A. Aktas et al., Eur. Phys. J. **C 40**, 349 (2005);
H1 Coll., A. Aktas et al., Eur. Phys. J. **C 45**, 23 (2006);
H1 Coll., A. Aktas et al., Preprint hep-ex/0605016, 2006.

[13] H1 Coll., A. Aktas et al., Phys. Lett. **B621**, 56 (2005).

[14] ZEUS Coll., S. Chekanov et al., *Measurement of open beauty production at HERA using a D^* + muon tag,* Contributed paper to this conference.

[15] ZEUS Coll., U. Holm (ed.), *The ZEUS Detector*. Status Report (unpublished), DESY (1993), available on `http://www-zeus.desy.de/bluebook/bluebook.html`.

[16] N. Harnew et al., Nucl. Inst. Meth. **A 279**, 290 (1989);
B. Foster et al., Nucl. Phys. Proc. Suppl. **B 32**, 181 (1993);
B. Foster et al., Nucl. Inst. Meth. **A 338**, 254 (1994).

[17] M. Derrick et al., Nucl. Inst. Meth. **A 309**, 77 (1991);
A. Andresen et al., Nucl. Inst. Meth. **A 309**, 101 (1991);
A. Caldwell et al., Nucl. Inst. Meth. **A 321**, 356 (1992);
A. Bernstein et al., Nucl. Inst. Meth. **A 336**, 23 (1993).

[18] G. Abbiendi et al., Nucl. Instr. and Meth. **A 333**, 342 (1993).

[19] ZEUS Coll., U. Holm (ed.), *The ZEUS Detector*. Status Report (unpublished), DESY (1993), available on `http://www-zeus.desy.de/bluebook/bluebook.html`.

[20] Tomasz Jezynski, Zbigniew Luszczak, Krzysztof T. Pozniak, Pawel Plucicinski, Grzegorz Grzelak, Krzysztof Kierzkowski, Maciej I. Kudla, Michal Pietrusinski, Proc. SPIE **5484**, 180 (2004).

[21] I. Bloch, *Measurement of beauty production from dimuon events at HERA / ZEUS*. Ph.D. Thesis, Hamburg University, Hamburg (Germany), Report DESY-THESIS-2005-034, DESY, 2005.

[22] W. H. Smith, K. Tokushuku and L. W. Wiggers, *Proc. Computing in High-Energy Physics (CHEP), Annecy, France, Sept. 1992*, C. Verkerk and W. Wojcik (eds.), p. 222. CERN, Geneva, Switzerland (1992). Also in preprint DESY 92-150B.

[23] ZEUS Coll., S. Chekanov et al., Nucl. Phys. **B729**, 492 (2005).

[24] T. Sjöstrand, Comp. Phys. Comm. **82**, 74 (1994).

[25] H. Jung, Comp. Phys. Comm. **86**, 147 (1995).

[26] G. Marchesini et al., Comp. Phys. Comm. **67**, 465 (1992).

[27] Abe, Tetsuo, Comput. Phys. Commun. **136**, 126 (2001).

[28] R. Brun et al., GEANT3, Technical Report CERN-DD/EE/84-1, CERN, 1987.

[29] A. Longhin, *Measurement of beauty production at HERA with a $D^* + \mu$ tag.* Ph.D. Thesis, Università di Padova, Padova (Italy), Report DESY-THESIS-2004-050, Università di Padova and INFN, 2004.

[30] G.M. Briskin, *Diffractive Dissociation in ep Deep Inelastic Scattering.* Ph.D. Thesis, Tel Aviv University, Report DESY-THESIS 1998-036, 1998.

[31] J. Binnewies, B.A. Kniehl and G. Kramer, Z. Phys. **C 76**, 677 (1997);
B.A. Kniehl, G. Kramer and M. Spira, Z. Phys. **C 76**, 689 (1997);
J. Binnewies, B.A. Kniehl and G. Kramer, Phys. Rev. **D 48**, 014014 (1998).

[32] A. Lipatov and N. Zotov, Preprint hep-ph/0601240, 2006;
A. Lipatov and N. Zotov, Preprint hep-ph/0603017, 2006;
H.Jung, Phys. Rev. **D 65**, 034015 (2002);
H.Jung, J. Phys. **G 28**, 971 (2002).

[33] CTEQ Coll., H.L. Lai et al., Eur. Phys. J. **C 12**, 375 (2000).

[34] M. Glück, E. Reya, and A. Vogt, Phys. Rev. **D46**, 1973 (1992).

[35] Adriana Elizabeth Nuncio-Quiroz, ZEUS Coll., talk at XIV International Workshop on Deep Inelastic Scattering, Tsukuba, Japan, 20-24 April 2006; to appear in proceedings, April 2006.

[36] T. Sjöstrand, L. Lönnblad, and S. Mrenna, Preprint hep-ph/0108264, 2001.

[37] S. Frixione and B.R. Webber, JHEP **06**, 029 (2002);
S. Frixione, P. Nason and R.B. Webber, JHEP **08**, 007 (2003).

[38] C. Peterson et al., Phys. Rev. **D 27**, 105 (1983).

[39] B. Andersson, G. Gustafson and B. Söderberg, Z. Phys. **C20**, 317 (1983);
B.R. Webber, Nucl. Phys. **B 238**, 492 (1984);
T. Sjöstrand, Comp. Phys. Comm. **39**, 347 (1986).

[40] Particle Data Group, K. Hagiwara et al., Phys. Rev. **D 66**, 010001 (2002).

[41] C.F. von Weizsäcker, Z. Phys. **88**, 612 (1934). In German;
E.J. Williams, Phys. Rev. **45**, 729 (1934);
S. Frixione et al., Phys. Lett. **B319**, 339 (1993).

	low inv. mass ($m_{\mu\mu} < 4$ GeV)	high inv. mass ($m_{\mu\mu} \geq 4$ GeV)
unlike-sign $\pm/\mp$	**muons from same b**, J/ψ, ψ' + light-flavour bg	**muons from different b** or c, Υ, Bethe Heitler + light-flavour bg
like-sign $++/--$	**light-flavour background**, + few muons from different b	**muons from different b** + light-flavour background

Table 1: *Grouping of events using dimuon mass and charge correlations. The main contributions of types of events are given.*

channel	effective branching fraction w/o $B^0\bar{B}^0$ mixing
$b \to \mu^-$ direct	10.95 ± 0.27 %
$b \to \mu^+$ indirect	8.27 ± 0.40 %
$b \to \mu^-$ indirect	2.21 ± 0.50 %
all $b \to \mu^\pm$	21.43 ± 0.70 %
$b\bar{b} \to \mu^\pm\mu^\mp$ (diff. b's)	2.42 ± 0.17 %
$b\bar{b} \to \mu^\pm\mu^\pm$ (diff. b's)	2.18 ± 0.14 %
$b \to \mu^+\mu^-$ all	2.40 ± 0.16 %

Table 2: *Effective branching fractions assumed for cross section determinations. The indirect contributions include cascade decays into muons via charm, anticharm, $\tau^\pm$ and J/ψ. The additional effect of $B^0\bar{B}^0$ mixing ($\chi = 0.1257 \pm 0.0042$) is not yet included.*

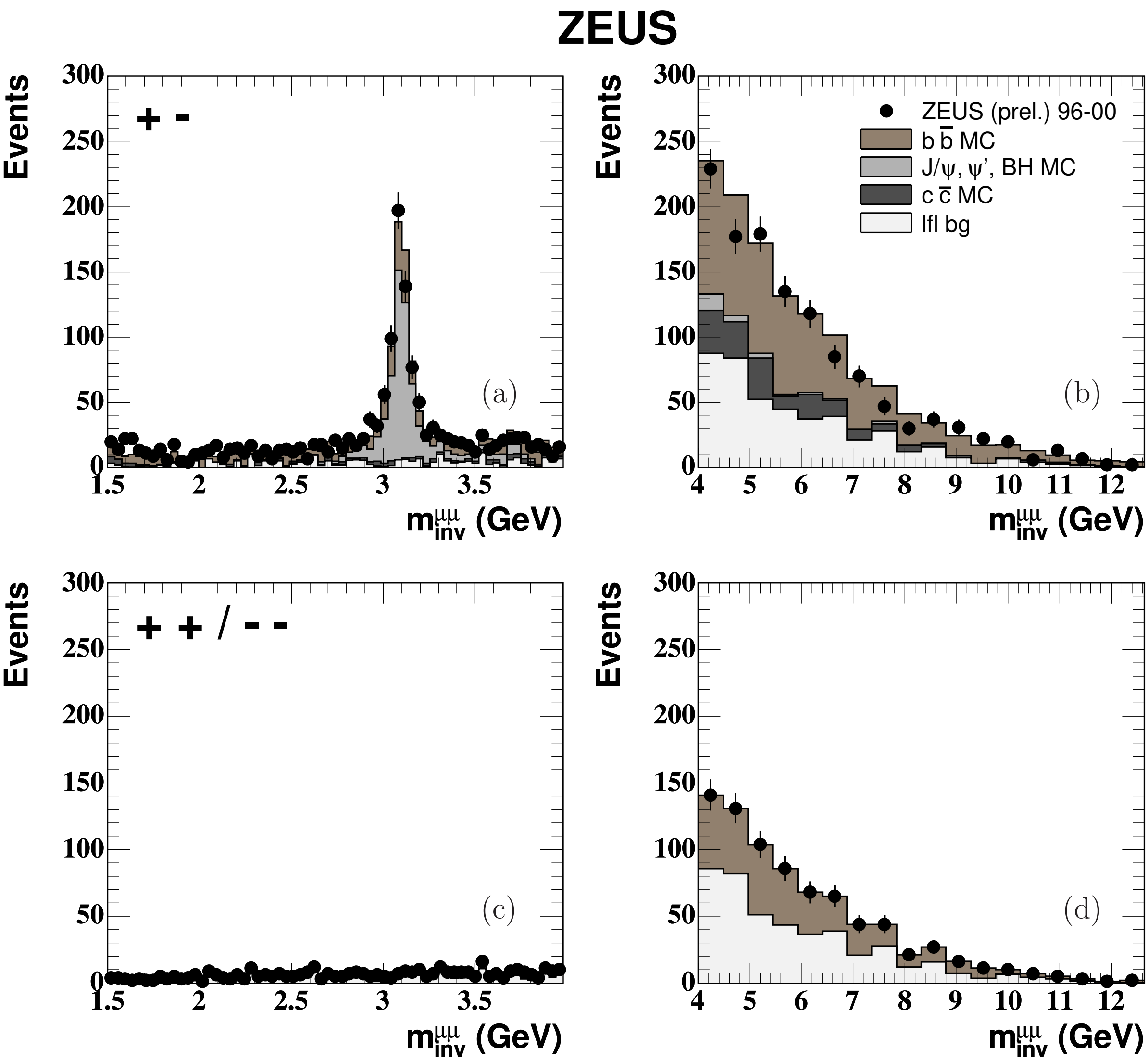

Figure 1: *Dimuon mass distributions of unlike sign dimuon pairs in the (a) low mass and (b) high mass subsamples, as well as like sign dimuon pairs in the (c) low and (d) high mass subsamples. The same vertical scale has been chosen for the like and unlike sign subsamples. The breakdown into the expected contributions from different processes is also shown.*

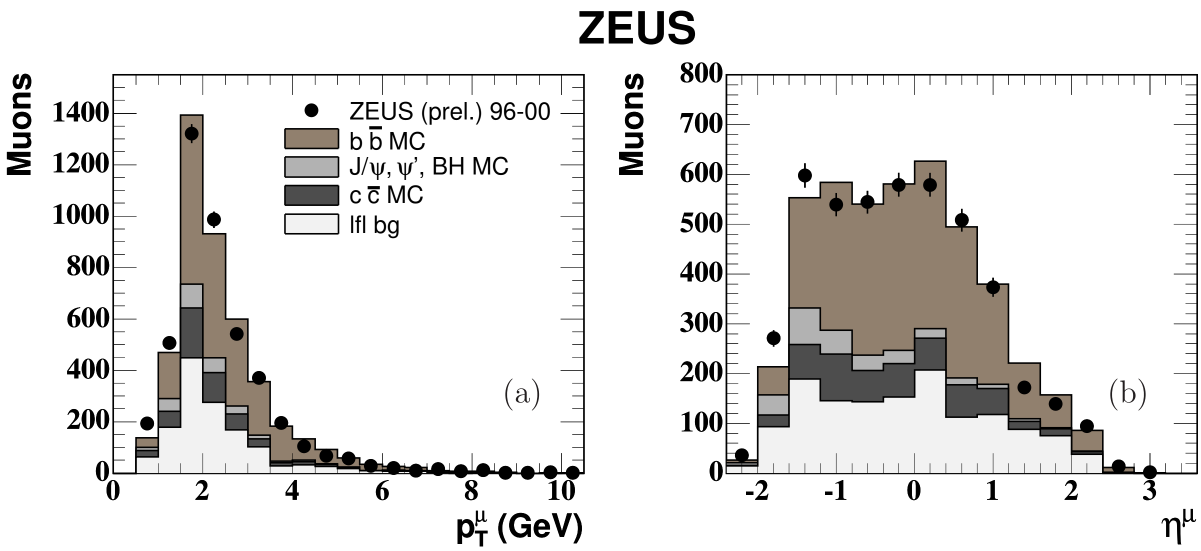

Figure 2: *Muon (a) transverse momentum and (b) pseudorapidity distribution from both high and low mass dimuon pairs in the nonisolated unlike sign sample. Two muons are entered for each event. The breakdown into the expected contributions from different processes is also shown.*

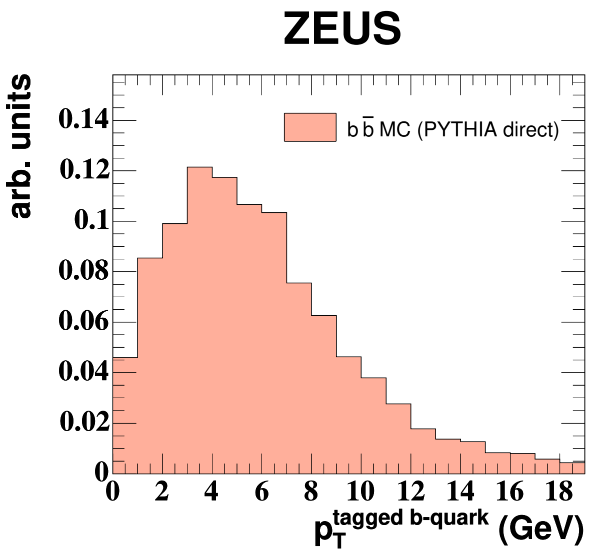

Figure 3: *Example of b quark transverse momentum distribution for quarks tagged by reconstructed muons in dimuon events, from PYTHIA direct processes.*

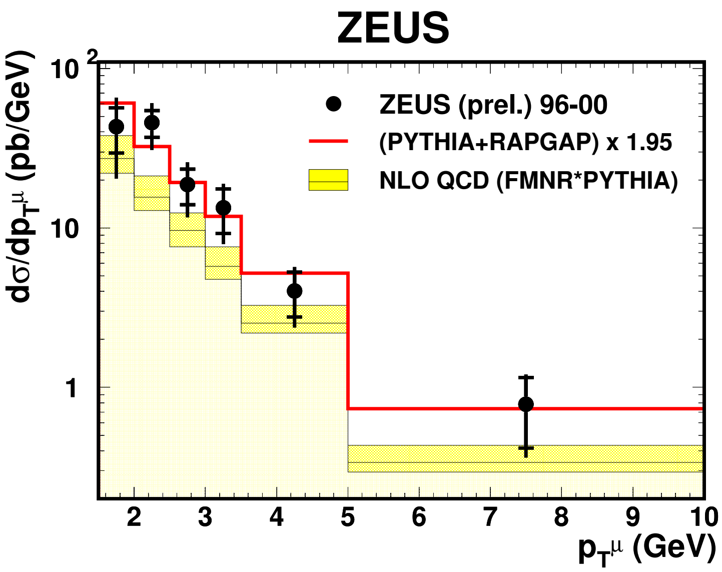

Figure 4: *Cross-section $d\sigma/dp_T^\mu$ for muons from b decays in dimuon events with $p_T^\mu > 1.5$ GeV and $-2.2 < \eta^\mu < 2.5$ for both muons. Two muons contribute for each event. The data (solid dots) are compared to the scaled sum of the predictions by the LO+PS generators PYTHIA and RAPGAP (histogram) and to the NLO QCD predictions from FMNR$\otimes$*PYTHIA *(band).*

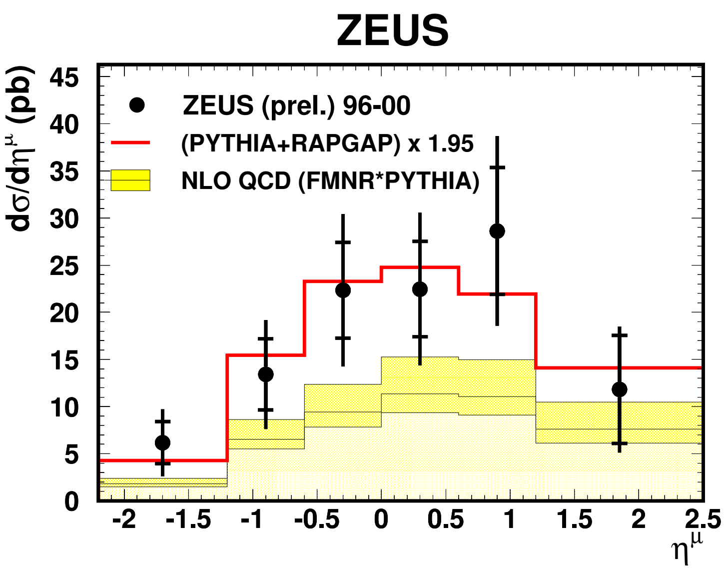

Figure 5: *Cross-section $d\sigma/d\eta^\mu$ for muons from b decays in dimuon events with $p_T^\mu > 1.5$ GeV and $-2.2 < \eta^\mu < 2.5$ for both muons. Two muons contribute for each event. The data (solid dots) are compared to the scaled sum of the predictions by the LO+PS generators PYTHIA and RAPGAP (histogram) and to the NLO QCD predictions from FMNR$\otimes$*PYTHIA *(band).*

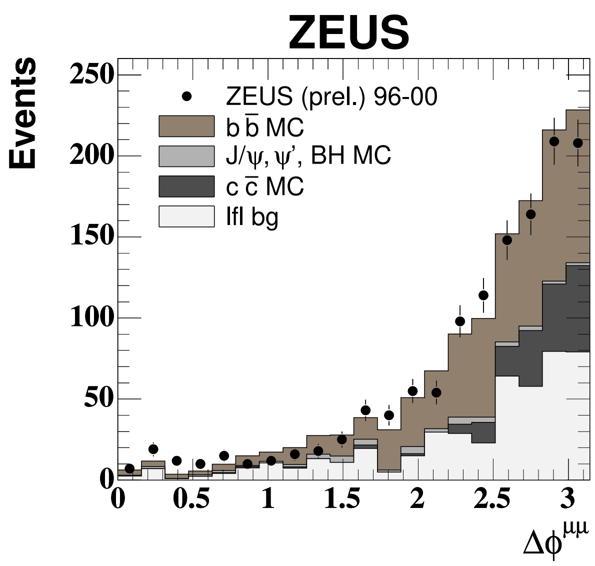

Figure 6: *Distribution of the azimuthal distance $\Delta\phi$ between the two muons in dimuon events with $p_T^\mu > 1.5$ GeV and $-2.2 < \eta^\mu < 2.5$ for both muons, and $m^{\mu\mu} > 3.25$ GeV. The breakdown into the expected contributions from different processes is also shown.*

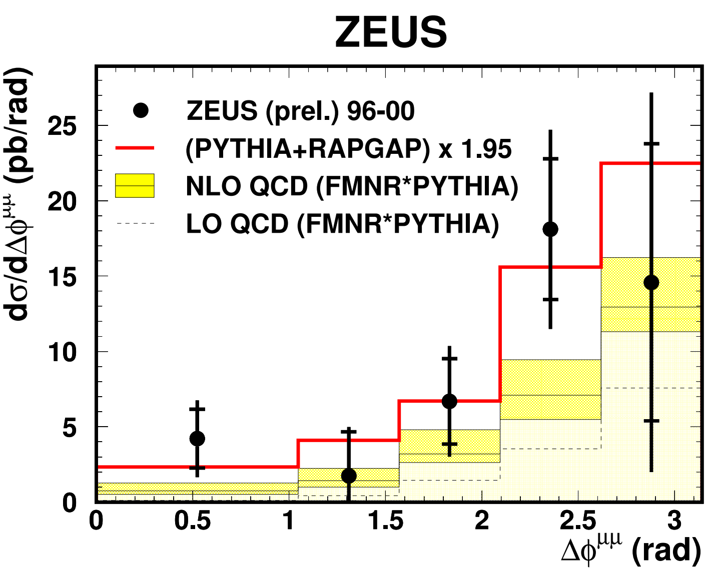

Figure 7: *Cross-section $d\sigma/d\Delta\phi^{\mu\mu}$ for dimuon events from $b\bar{b}$ decays in which each muon originates from a different $b(\bar{b})$ quark, with $p_T^\mu > 1.5$ GeV and $-2.2 < \eta^\mu < 2.5$ for both muons. The data (solid dots) are compared to the scaled sum of the predictions by the LO+PS generators PYTHIA and RAPGAP (histogram) and to the LO (dashed line) and NLO (band) QCD predictions from FMNR$\otimes$*PYTHIA.

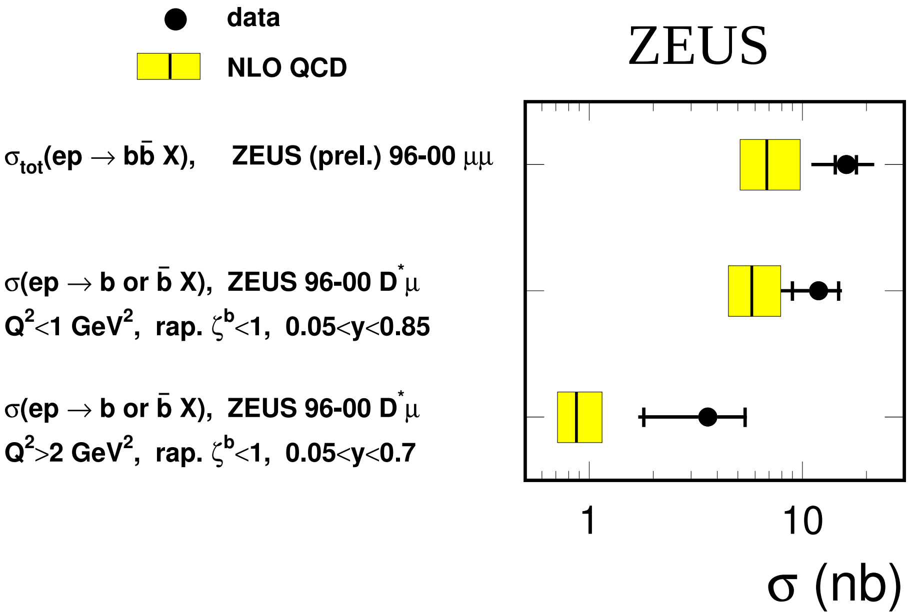

Figure 8: *Comparison of measured cross sections to NLO predictions. The $b\bar{b}$ cross section from this analysis is shown at the top. For comparison, related b or $\bar{b}$ cross sections obtained in the ZEUS $D^*\mu$ analysis for the photoproduction regime (middle line) and DIS (lower line), are also shown.*

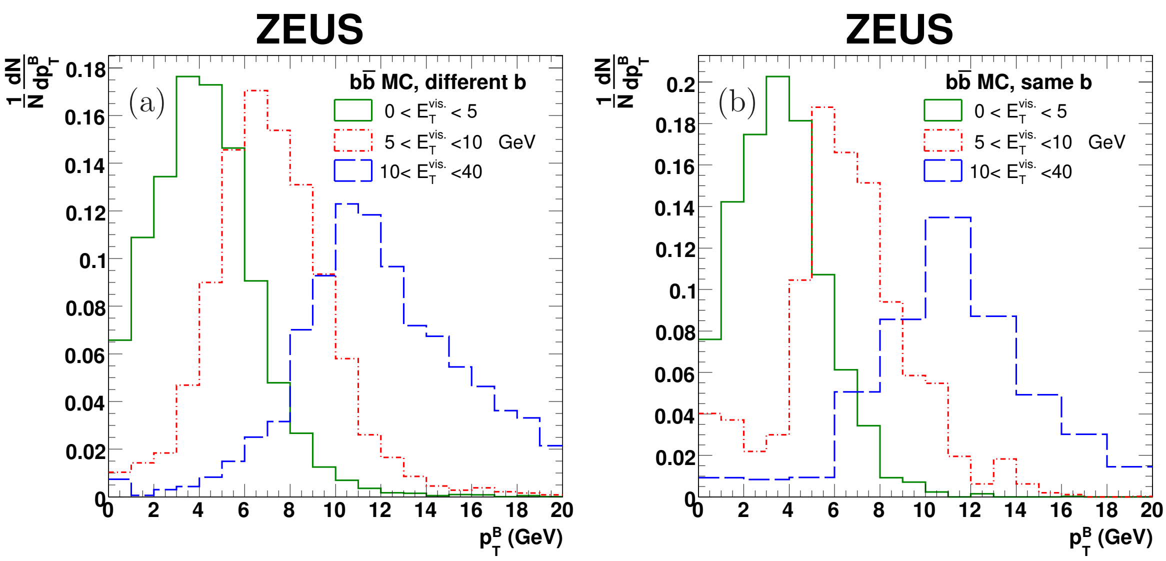

Figure 9: *Distribution of the p_T of the parent B hadron for muons from different b quarks (a) or from the same b quark (b), for the three E_T^{vis} bins indicated in the figures.*

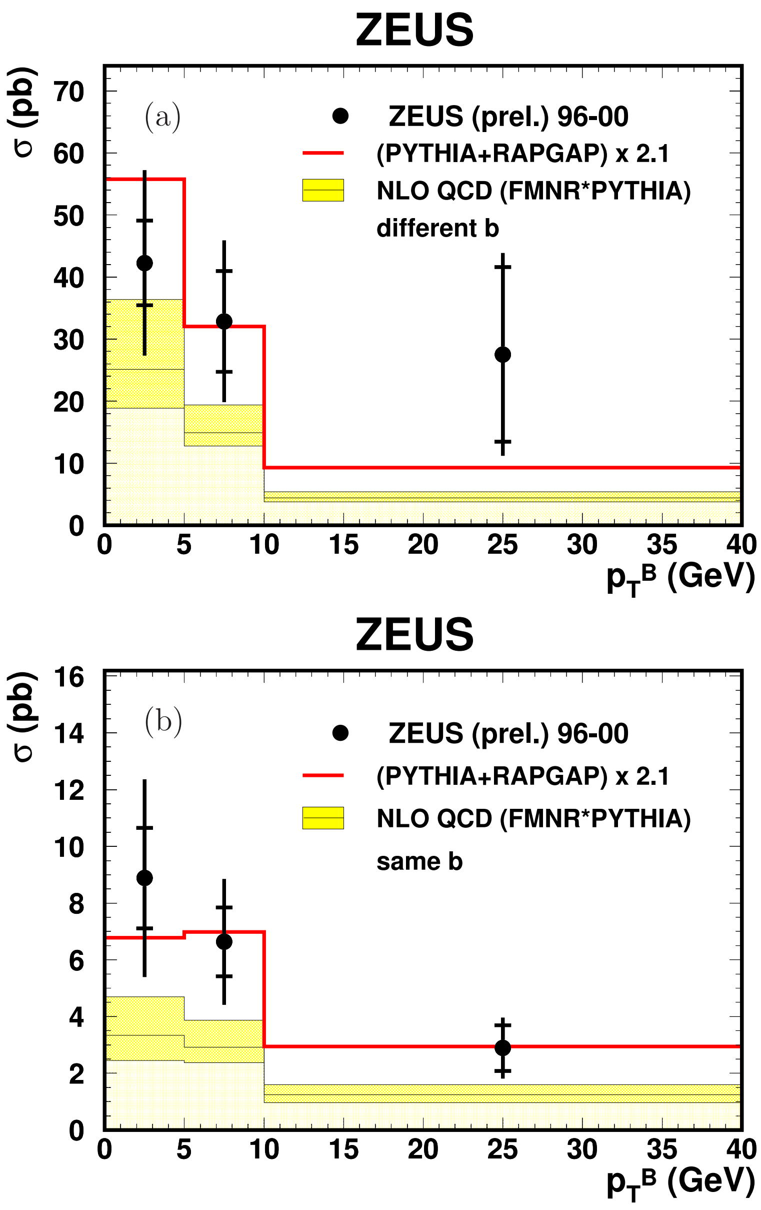

Figure 10: *Visible cross section for parent B hadrons from events containing two muons satisfying the cuts for the total cross section measurement (18), and in which both muons originate from a different (a) or from the same $b(\bar{b})$ quark (b), in three bins of p_T^B. There are two entries per event for (a), and one entry per event for (b). The data (solid dots) are compared to the scaled sum of the predictions by the LO+PS generators PYTHIA and RAPGAP (histogram) and to the NLO QCD predictions from FMNR⊗*Pythia *(band).*

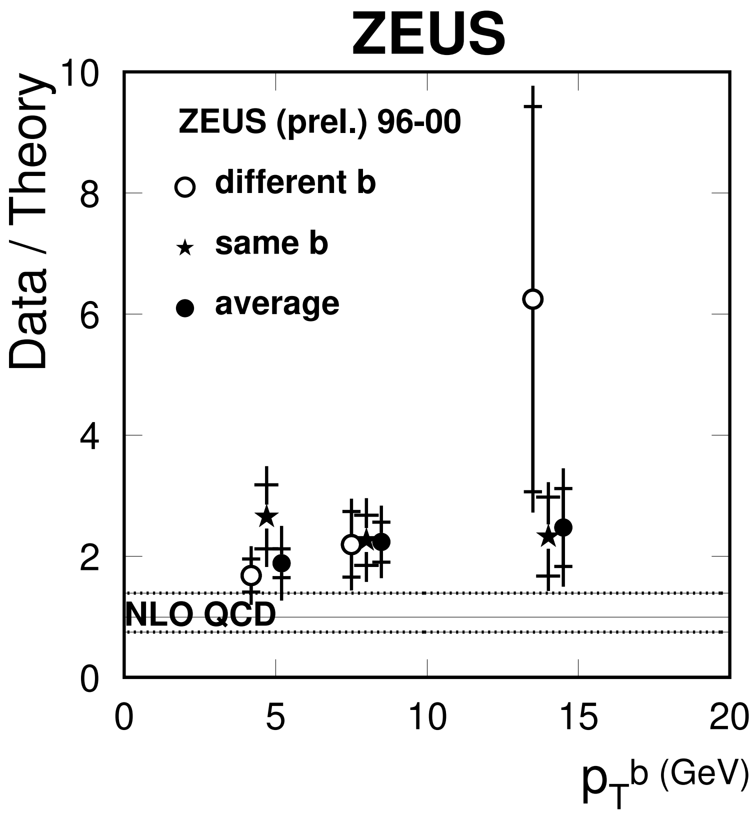

*

Figure 11: *Data/NLO ratio for cross sections from different b quarks (open circles) compared to measurements from the same b quark (stars) and their average (filled circles). The value for each E_T^{vis} (or p_T^B) interval (0-5,5-10,10-40 GeV) is quoted at the median p_T of the parent b quarks in events satisfying all detector level cuts (4.7,8.0,14.0 GeV). The different b and average points are shown slightly shifted in p_T^B for clarity. The NLO error band slightly depends on the kinematic cuts of each point and is approximate only.*

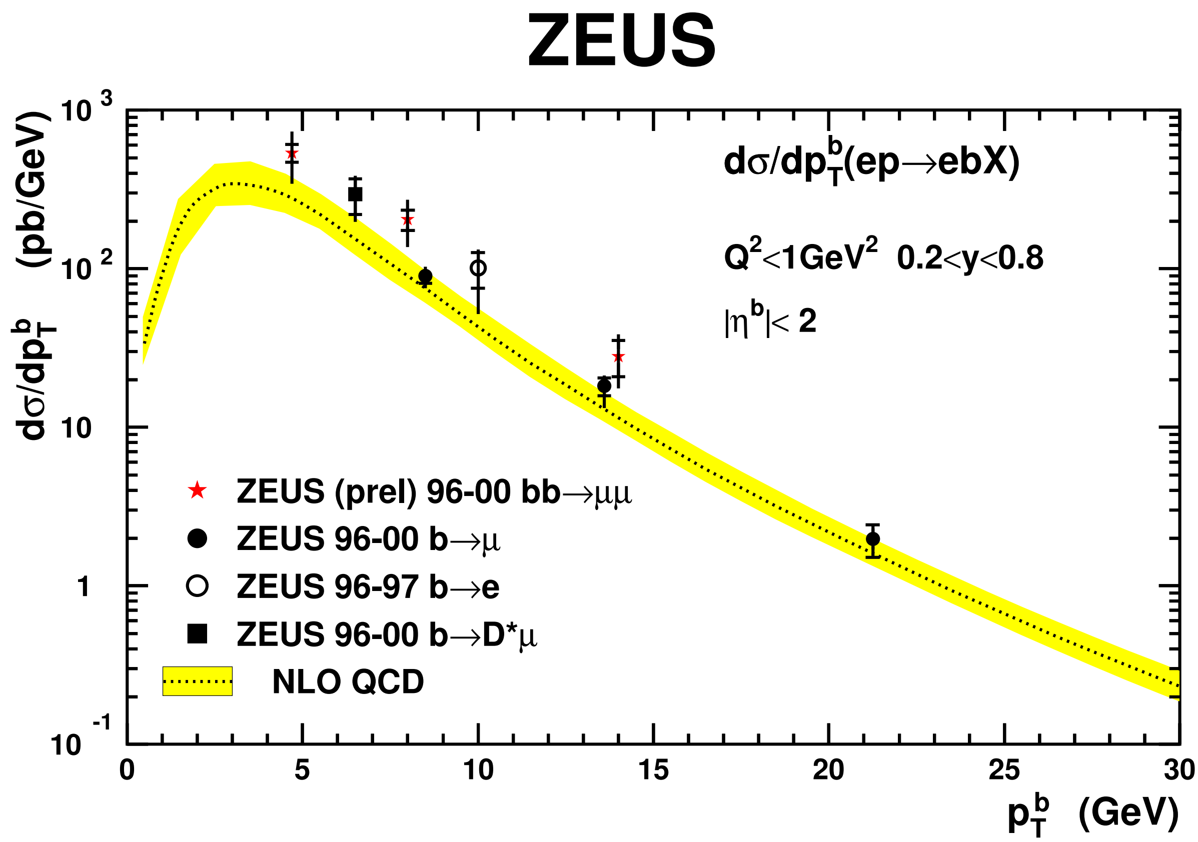

Figure 12: *Differential cross section $\frac{d\sigma}{dp_T^b}$ of this analysis (stars) compared to previous ZEUS measurements (other symbols) and NLO (band), after rescaling to the kinematic range indicated in the figure.*